Materials International
Open Access Journal (ISSN: 2668-5728)

Article
Volume 6, Issue 2, 2024, 17
https://doi.org/10.33263/Materials62.017

Insight into Inhibition Efficiencies of Mannich Bases of Thiourea Derivatives for Mild Steel Corrosion in 0.5 M Sulphuric Acid Medium- An Experimental and Theoretical Approach

Lavanya D. Kateel [1,*], Priya V. Frank [2], Vijaya D.P. Alva [3], Supriya Bangera [4]

1. Department of Chemistry, Canara Engineering College, Benjanapadavu -574219 and affiliated to Visvesvaraya Technological University, Belagavi, Karnataka
2. Department of Chemistry, Canara Engineering College, Benjanapadavu -574219 and affiliated to Visvesvaraya Technological University, Belagavi, Karnataka
3. Department of Chemistry, Shree Devi Institute of Technology, Mangaluru, and affiliated to Visvesvaraya Technological University, Belagavi, Karnataka
4. Department of Chemistry, P.A. College of Engineering Nadupadavu Mangaluru- 574153 and affiliated to Visvesvaraya Technological University, Belagavi, Karnataka

* Correspondence: lavanyakateel@gmail.com;

Scopus Author ID 57216254744

Received: 25.02.2024; Accepted: 12.05.2024; Published: 10.06.2024

Abstract: The inhibition efficiency of the mannich bases 1-[(4-methylpiperazin-1-yl)(phenyl)methyl]thiourea and 1-[(4-ethylpiperazin-1-yl)(phenyl)methyl]thiourea for mild steel corrosion tested in 0.5 M sulphuric acid medium in the temperature range 303 K to 333 K was assessed by electrochemical impedance spectroscopy, potentiodynamic polarisation measurement and density functional theory techniques. The surface morphology of the uninhibited and inhibited mild steel samples was analyzed using Scanning Electron Microscopy (SEM) and energy-dispersive X-ray spectroscopy (EDX). UV-visible spectroscopy and IR analysis of the corrosion product were performed to know the interaction of inhibitors with the mild steel surface. From the electrochemical studies, it is evident that the inhibition efficiency of both inhibitors increased with the increase in the concentration of both inhibitors but decreased with the increase in the temperature. The adsorption inhibitors on the metal surface are an exothermic process and follow Langmuir's adsorption isotherm. The adsorption is a mixed type adsorption that involves both chemisorption and physisorption. The results obtained by the DFT study are well correlated with the results of experimental studies.

Keywords: corrosion inhibitors; polarization; electrochemical impedance; mannich base.

1. Introduction

Mild steel is one of the most commonly used metals in various industries due to its excellent mechanical properties and low cost. However, mild steel undergoes severe corrosion in the presence of acid solution used during the boilers' cleaning and removal of mild steel scale [1]. Corrosion of mild steel can be effectively prevented by using corrosion inhibitors. Organic inhibitors such as Mannich bases containing nitrogen, oxygen, sulfur, and π-electrons are found to be very efficient inhibitors for the corrosion of mild steel in an acid medium because of their capability to get adsorbed onto the metal surfaces [2, 3]. The study of Mannich bases has gained the highest importance because of its high inhibition efficiency, easy synthesis, and low cost.

In the present work, Mannich bases such as 1-[(4-methylpiperazin-1-yl)(phenyl)methyl]thiourea(MPPMT) and 1-[(4-ethylpiperazin-1-yl)(phenyl)methyl]thiourea (EPMT)(Figure 1) which were synthesized easily from relatively cheap raw materials and are tested as a corrosion inhibitor in 0.5 M sulphuric acid medium at different temperatures. The synthesis and characterization of these inhibitors were discussed in our earlier publication [4].

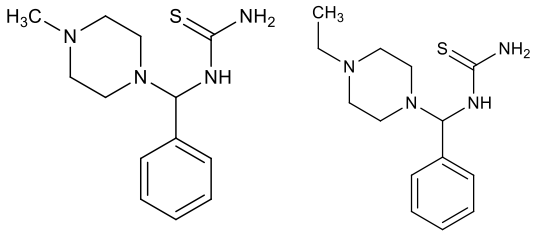

MPPMT EPMT

Figure 1. Molecular structure of Mannich Bases.

2. Materials and Methods

2.1. Preparation of electrode surface.

The experiments were carried out using an MS sample with chemical composition (wt%) C(0.18), Mn(0.6), Si(0.1), P(0.04), and remainder Fe(99.03). The mild steel cylindrical test sample was cut from the rod and covered with cold-setting resin, and a surface area of 1 cm^2 was exposed to the corrosive medium. The test specimen was subjected to belt grinding and polished using emery paper of different grades, followed by a mirror polishing on a disk polishing wheel with levigated alumina. The MS sample was cleaned with distilled water and acetone, dried with tissue paper, and immersed in a corrosive medium.

2.2. Preparation of corrosive medium.

The 0.5 M sulphuric acid solution was prepared by diluting AR grade 98 % sulphuric acid with distilled water. To check the exact concentration of the acid solution, the prepared solution was titrated against sodium hydroxide, which was standardized using oxalic acid. The efficiencies of the inhibitors were also studied by preparing various concentrations of inhibitors ranging from 50–1000 ppm in 0.5 M sulphuric acid at various temperatures in the range 303-333 K.

2.3. Electrochemical study.

All electrochemical tests were conducted using the electrochemical work station, Gill AC 1864 of ACM instruments, England. Conventional three-electrode cell assemblies with platinum as a counter electrode, saturated calomel electrode as a reference electrode, and mild steel as a working electrode (SCE) were used for electrochemical experiments. The specimen was finely polished and immersed in 0.5 M sulphuric acid containing various concentrations of inhibitors. After the attainment of open circuit potential, all the measurements were recorded.

2.3.1. Electrochemical impedance study.

The Electrochemical Impedance spectroscopy tests were carried out by applying a 10 mV amplitude of AC signal in the 100 kHz–0.01 Hz frequency spectrum on the OCP. The

Nyquist plots were used to analyze the impedance data and fitted to appropriate circuits using ZSimpWin version 3.21 software.

2.3.2. Potentiodynamic polarization study.

Potentiodynamic studies were done immediately after the EIS studies with the same specimen in the same medium. The potentiodynamic current–potential curves were recorded from -250 mV to +250 mV for the OCP at a 1 mV /s scan rate.

2.4. UV-visible spectral analysis.

The UV–Visible spectra of the 1000 ppm of both MPPMT and EPMT inhibitors in 0.5M sulphuric acid solution were taken at room temperature using UV–Visible absorption spectrophotometer (Shimadzu UV-1800 Japan) in the wavelength range 190-800 nm. Later, absorption spectra of 1000 ppm of both the inhibitors in 0.5 M sulphuric acid were obtained after a mild steel specimen was immersed for 22 hours. Then, they were used to explain the mechanism of inhibition.

2.5. FT-IR spectroscopy.

FT-IR studies were performed for MS samples exposed to 0.5 M sulphuric acid, without and with optimum concentration of inhibitors. After immersing the mild steel specimen for 22 hours in the corrosive medium under optimum inhibitor concentration at room temperature, the surface layer of the specimen was scratched, and the collected powder was dried. This powder was subjected to analysis using a Fourier Transform Infrared Spectrometer (IRPrestige-21, Shimadzu, Japan).

2.6. Surface morphology study.

The morphological study of the mild steel in the absence and presence of the inhibitor in 0.5 M sulphuric acid was studied with the help of a scanning electron microscope (CARLZEISS 03-81 Germany). Elemental analysis was done using an energy-dispersive X-ray spectroscopy (EDX) technique using an Oxford instrument after 22 hours of immersion in 0.5 M sulphuric acid with 1000 ppm of inhibitors at 303K.

2.7. Quantum chemical calculation.

The reactivity parameters and electron binding ability of inhibitor molecules MPMT and EPMT were studied by density functional theory using Gaussian 03 W software. The optimized structure obtained energies of the highest occupied orbital (EHOMO) and lowest occupied orbital (ELUMO). These were used to calculate other quantum parameters like energy gap(ΔE)**,** ionization potential (I), chemical potential (μ), electron affinity (A), Chemical softness or electron polarizability (σ,) chemical hardness (η), electrophilicity index (ω) and electronegativity (χ).

3. Results and Discussion

3.1. Electrochemical studies.

3.1.1. Electrochemical impedance spectroscopy (EIS) study.

EIS measurements were carried out for various concentrations of MPPMT and EPMT inhibitors in the temperature range of 303 K to 333 K after attaining the open circuit potential. To obtain the steady state, the mild steel specimen was immersed for 30 minutes in 0.5 M sulphuric acid with different concentrations of inhibitors before the electrochemical studies [5]. After 30 minutes, open circuit potential is recorded as a function of time for 400 s. Figure 2 shows the steady-state OCP curves for the mild steel sample in 0.5 M sulphuric acid with different concentrations of both MPPMT and EPMT inhibitors. Nyquist plots obtained for mild steel in 0.5 M sulphuric acid at different inhibitor concentrations at 303 K are shown in Figure 3.

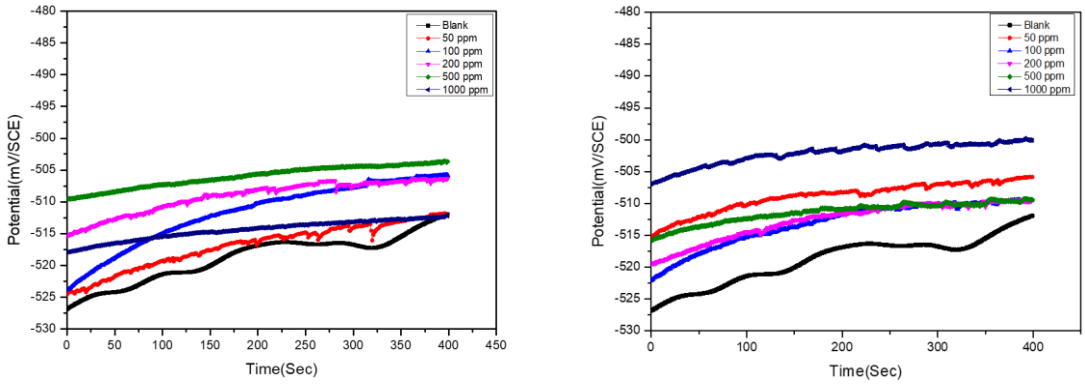

Figure 2. Variation of open circuit potential with time for MS in 0.5 M sulphuric acid with various concentrations of **(a)** MPPMT; **(b)** EPMT.

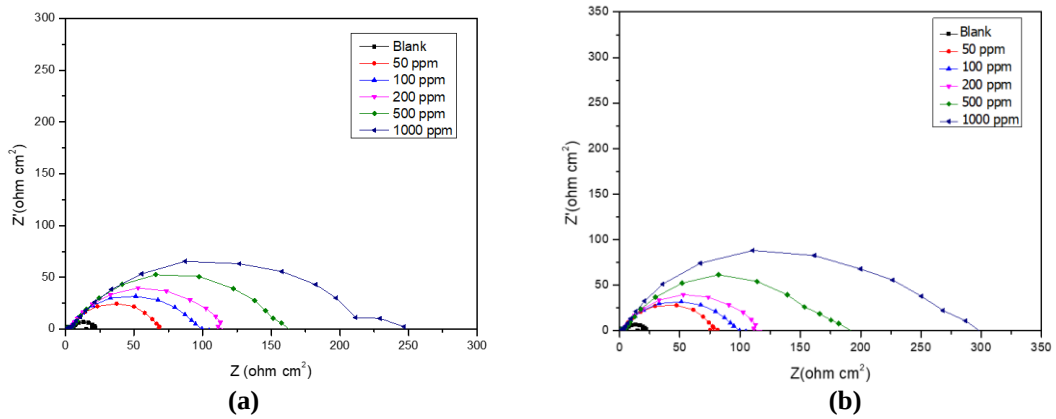

Figure 3. Nyquist plots of MS in 0.5 M sulphuric acid with various concentrations of **(a)** MPPMT; **(b)** EPMT at 303 K.

It is observed that in Nyquist plots, the radius of the semicircle increased with a rise in the concentration of both MPPMT and EPMT inhibitors, which gives proof for the adsorbing capacity of the inhibitor [6]. The shape of the Nyquist plots remains the same in the unprotected and protected system of mild steel surface in an acid medium, showing no change in the corrosion inhibition mechanism. In the present study, the Nyquist plot appears to be a depressed semicircle. This can be due to surface roughness, electrode irregularity, and electrode surface non-homogeneity [7].

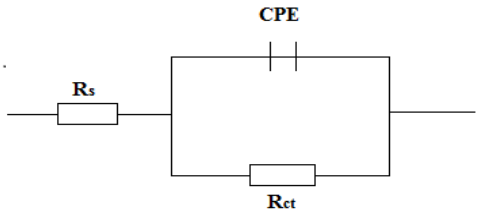

Figure 4. An equivalent circuit diagram is used to fit EIS data.

The impedance parameters are obtained by fitting the impedance spectra with an equivalent circuit[R(QR)] Figure 4, and the circuit is composed of a solution resistance component (R_s), a charge transfer resistance (R_{ct}), and a constant phase element (CPE)[8]. The impedance function of the element is represented by Eq. (1).

$$Z = Y_o^{-1}(iw)^{-n} \qquad (1)$$

where Y_o is the proportionality factor representing the CPE magnitude, i is the imaginary number, w is the angular frequency, and n is the exponent related to the phase shift indicating the degree of surface roughness [9, 10]. The double-layer capacitance C_{dl} values were obtained from charge transfer resistance R_{ct} and constant phase element parameters (Y_o and n) as per Eq. (2). The C_{dl} values reduced with an increase in the inhibitor concentration in most of the cases as a result of the increase in the thickness of the protective film and reduction in local dielectric constant [11]. The irregular trend in C_{dl} values suggests the complexity of the adsorption-desorption process [12].

$$C_{dl} = [Y_o(R_{ct})^{1-n}]^{1/n} \qquad (2)$$

From Tables 1a and 1b, it is clear that the R_{ct} value increases with a rise in the concentration of MPPMT and EPMT inhibitors. The high R_{ct} values suggest the formation of a protective layer on the surface of the metal, thereby reducing the rate of corrosion.

From the R_{ct} values, the percentage of IE is obtained according to Eq. (3).

$$\eta(\%) = \frac{(R_{ct(inh)} - R_{ct})}{R_{ct}} \times 100 \qquad (3)$$

where $R_{ct(inh)}$ and R_{ct} are the charge transfer resistances in the presence and absence of an inhibitor, respectively.

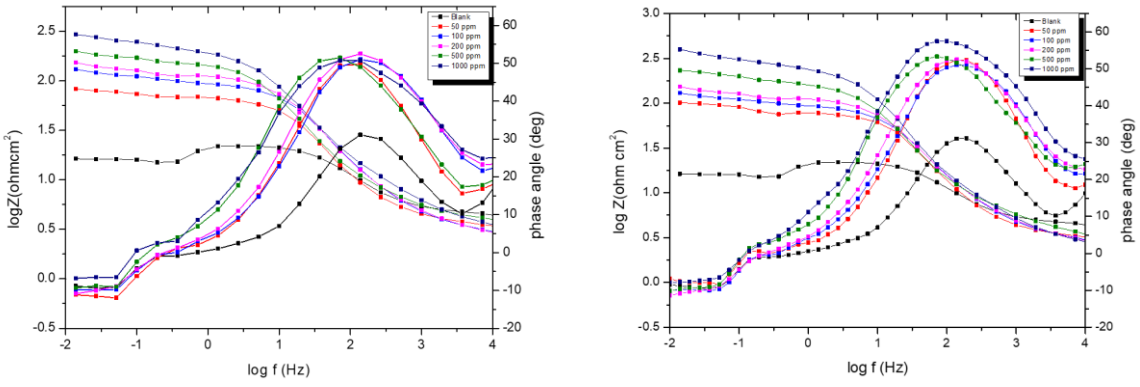

(a) **(b)**

Figure 5. Bode plots of MS in 0.5 M sulphuric acid with varying concentrations of **(a)** MPPMT; **(b)** EPMT at 303 K

The Bode plots of MS immersed in 0.5 M sulphuric acid without and with varying concentrations of MPPMT and EPMT at 303 K are depicted in Figures 5a and 5b. Bode impedance plots show that adding inhibitors to a corrosive medium increases the surface smoothness of the metal. As per the literature [13], an ideal capacitor has an ideal phase angle and a constant slope value of -90° and -1. The current study's ideal capacitive behavior change

is caused by surface roughness [14]. The Bode plots with and without inhibitors demonstrate that deviation from ideal capacitive behavior is more effective without inhibitors. The slope and phase angles are significantly increased because of the development of a protective coating on the MS surface in the presence of inhibitors. The decrease in the dissolution rate of the metal causes a rise in the phase angles as the concentration of the inhibitors increases [15].

The experimental results of electrochemical impedance spectroscopy, such as charge transfer resistance (R_{ct}), double-layer capacitance (C_{dl}), and the calculated values of IE% without and with an inhibitor in 0.5 M sulphuric acid at 303-333 K are tabulated in Table 1a and 1b.

Table 1. (a) Impedance parameters for MS corrosion in 0.5M sulphuric acid at various concentrations of MPPPMT at varying temperatures.

Temp (K)	Inhibitor Conc. (ppm)	R_s	R_{ct} (Ωcm^2)	$Q\times10^{-4}$ ($s^n/\Omega cm^2$)	n	C_{dl} (μFcm^{-2})	%IE
303K	Blank	4.627	17.09	3.504	0.8303	123	---
	50	3.443	66.53	3.365	0.794	125	74.31
	100	3.491	92.45	4.734	0.748	164	81.51
	200	3.662	94.63	4.302	0.761	157	81.94
	500	3.969	157.5	3.942	0.7484	154	89.14
	1000	3.137	229.5	3.860	0.6936	132	92.55
313K	Blank	4.003	12.3	3.383	0.8667	145	---
	50	3.671	26.15	4.612	0.7948	147	52.96
	100	3.733	36.00	8.421	0.7911	334	65.83
	200	3.494	58.15	6.397	0.7653	233	78.84
	500	3.625	92.14	5.150	0.7274	164	86.65
	1000	3.89	168.2	4.803	0.7369	195	92.68
323K	Blank	3.468	8.718	5.245	0.8154	154	---
	50	2.981	14.29	11.20	0.7916	377	38.99
	100	2.788	20.97	9.087	0.7708	279	58.42
	200	3.913	31.67	11.850	0.7571	413	72.47
	500	3.165	65.48	6.513	0.7867	276	86.68
	1000	3.557	106.7	7.060	0.7311	272	91.82
333K	Blank	2.634	4.71	19.96	0.7017	274	---
	50	2.813	5.635	18.95	0.7806	526	16.41
	100	3.505	7.898	18.04	0.7997	622	40.36
	200	3.274	12.28	20.37	0.7723	686	61.64
	500	3.674	27.75	16.25	0.7481	571	83.02
	1000	2.597	46.52	15.46	0.7077	521	89.87

Table 1. (b) Impedance parameters for MS corrosion in 0.5 M sulphuric acid at various concentrations of EPMT at varying temperatures.

Temp (K)	Inhibitor Conc. (ppm)	R_s	R_{ct} (Ωcm^2)	$Q\times10^{-4}$ ($s^n/\Omega cm^2$)	n	C_{dl} (μFcm^{-2})	%IE
303K	Blank	4.627	17.09	3.504	0.8303	123	---
	50	3.140	76.99	2.354	0.8079	90	77.80
	100	2.764	99.93	3.051	0.7473	93	82.89
	200	2.779	117.4	2.971	0.7486	96	85.44
	500	3.588	181.5	3.265	0.743	122	90.58
	1000	2.609	282.1	2.386	0.7501	97	93.94
313K	Blank	4.003	12.3	3.383	0.8667	145	---
	50	3.511	30.08	4.145	0.7932	132	59.10
	100	3.413	71.49	2.676	0.8074	104	82.79
	200	3.286	86.00	4.125	0.7682	150	85.69
	500	3.625	99.41	6.076	0.793	292	87.62
	1000	2.65	244.9	3.080	0.8025	160	94.97
323K	Blank	3.468	8.718	5.245	0.8154	154	---
	50	3.624	20.49	4.787	0.8057	156	57.45
	100	3.434	27.07	6.108	0.7942	210	67.79
	200	3.04	44.71	6.285	0.7494	190	80.50

Temp (K)	Inhibitor Conc. (ppm)	R_s	R_{ct} (Ωcm^2)	$Q \times 10^{-4}$ ($s^n/\Omega cm^2$)	n	C_{dl} ($\mu F cm^{-2}$)	%IE
	500	3.318	70.73	1.950	0.7514	47	87.67
	1000	4.005	136.00	6.092	0.7596	277	93.58
333K	Blank	2.634	4.710	20.00	0.7020	274	---
	50	3.246	6.622	17.83	0.7671	463	28.87
	100	3.141	9.075	7.433	0.8276	262	48.09
	200	4.016	15.82	12.43	0.7966	455	70.22
	500	3.978	30.7	14.84	0.7629	568	84.65
	1000	3.386	60.82	13.55	0.7356	552	92.25

3.1.2. Potentiodynamic polarisation measurement.

The potentiodynamic polarization curves for mild steel in 0.5 M sulphuric acid solution were plotted in the absence and presence of varying concentrations of MPMT and EPMT at 303 K, as shown in Figure 6. The electrochemical parameters such as corrosion potential (E_{corr}), corrosion current density (i_{corr}), corrosion rate (υ_{corr}), cathodic and anodic Tafel slopes (β_c and β_a) are obtained from the polarization curve.

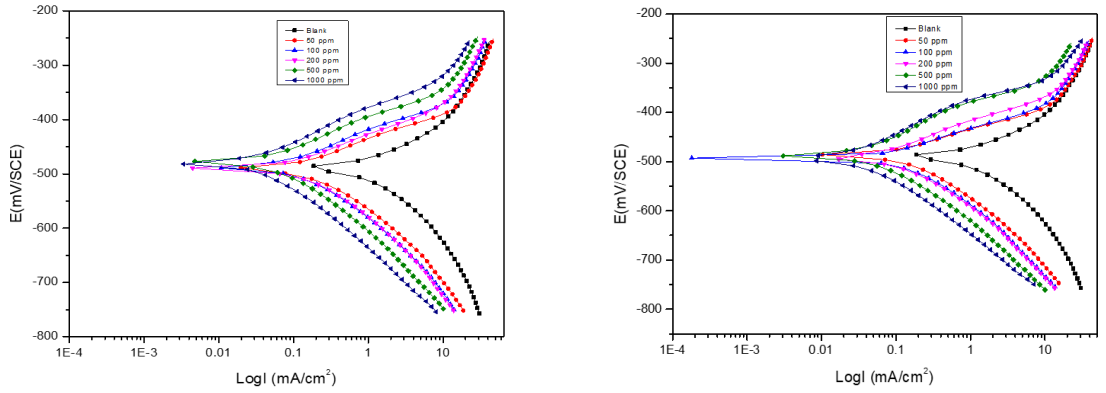

Figure 6. Tafel curves of MS in 0.5M sulphuric acid at varying concentrations of **(a)** MPPMT; **(b)** EPMT at 303K.

The inhibitor's percentage inhibition efficiency may be calculated using Eq. (4).

$$\eta(\%) = \frac{i_{corr} - i_{corr(inh)}}{i_{corr}} x100 \qquad (4)$$

where i_{corr} and $i_{corr(inh)}$ are the corrosion current densities in the absence and in the presence of the inhibitors, respectively. The electrochemical corrosion parameters, such as corrosion potential (E_{corr}), corrosion current density (i_{corr}), and corrosion rate (υ_{corr}), obtained by extrapolation of Tafel lines, are tabulated in Tables 2a and 2b.

Table 2. (a) Results of polarization method for MS corrosion in 0.5M sulphuric acid at varying concentrations of MPPMT at 303-333K.

Temp (K)	Conc. of inhibitor (ppm)	E_{corr} (mV/SCE)	β_a ($mVdec^{-1}$)	$-\beta_c$ ($mVdec^{-1}$)	i_{corr} ($mA.cm^{-2}$)	CR ($mm\ y^{-1}$)	%IE
303	Blank	-489.68	100.71	155.52	1.4155	16.731	
	50	-490.64	71.04	143.66	0.3956	4.6769	72.04
	100	-488.27	73.96	143.89	0.2699	3.1912	80.92
	200	-490.01	74.43	139.49	0.2510	2.9669	82.26
	500	-478.82	71.65	143.21	0.1401	1.6566	90.09
	1000	-481.02	74.06	134.83	0.0722	0.8534	94.89
313	Blank	-478.89	115.82	196.63	2.5985	30.715	
	50	-489.75	81.40	173.20	1.2077	14.275	53.52
	100	-487.47	86.28	160.67	0.9262	10.948	64.35
	200	-486.75	81.76	146.94	0.5435	6.4241	79.08
	500	-490.4	86.29	145.01	0.3001	3.5477	88.44
	1000	-478.31	72.12	147.05	0.1668	1.9716	93.58
323	Blank	-477.66	130.56	227.92	4.1283	48.796	
	50	-487.09	109.30	205.47	2.6761	31.632	35.17

Temp (K)	Conc. of inhibitor (ppm)	E_{corr} (mV/SCE)	β_a ($mVdec^{-1}$)	$-\beta_c$ ($mVdec^{-1}$)	i_{corr} ($mA.cm^{-2}$)	CR ($mm\ y^{-1}$)	%IE
	100	-484.38	89.98	192.85	1.8699	22.102	54.70
	200	-486.72	98.52	165.74	1.3395	15.833	67.55
	500	-488.55	92.79	164.54	0.5909	6.9845	85.68
	1000	-484.25	84.93	168.31	0.3982	4.7075	90.35
333	Blank	-475.87	157.68	266.90	8.5191	100.69	
	50	-483.62	148.27	264.04	6.6865	79.034	16.41
	100	-485.64	142.32	232.22	4.6043	54.422	40.36
	200	-483.61	109.64	207.68	3.1163	36.272	61.64
	500	-486.44	105.38	159.40	1.5943	18.845	83.02
	1000	-486.34	89.68	159.75	0.8946	10.412	89.87

Table 2. (b) Results of polarization method for MS corrosion in 0.5 M sulphuric acid at varying concentrations of EPMT at 303-333K.

Temp (K)	Conc. of inhibitor (ppm)	E_{corr} (mV/SCE)	β_a ($mVdec^{-1}$)	$-\beta_c$ ($mVdec^{-1}$)	i_{corr} ($mA.cm^{-2}$)	CR ($mm\ y^{-1}$)	%IE
303	Blank	-489.68	100.71	155.52	1.4155	16.731	---
	50	-486.89	65.26	148.34	0.3283	3.8810	76.80
	100	-492.57	68.23	144.81	0.2529	2.9894	82.13
	200	-492.25	73.61	135.47	0.2041	2.4127	85.58
	500	-486.50	85.54	152.14	0.1487	1.7586	89.48
	1000	-493.31	76.17	134.65	0.0769	0.9092	94.56
313	Blank	-478.89	115.82	196.63	2.5985	30.715	---
	50	-484.04	78.22	154.13	1.1440	13.522	55.97
	100	-491.00	80.69	161.17	0.5166	6.1073	80.11
	200	-493.52	78.71	154.49	0.4457	5.2691	82.84
	500	-488.49	85.12	153.77	0.3588	4.2418	86.19
	1000	-465.60	76.86	160.72	0.1885	2.2285	92.74
323	Blank	-477.66	130.56	227.92	4.1283	48.796	---
	50	-482.52	92.385	197.03	2.0128	23.791	51.24
	100	-485.48	81.58	185.11	1.4212	16.798	65.57
	200	-491.01	90.82	174.32	0.9824	11.612	76.20
	500	-486.67	93.18	148.31	0.6078	7.1844	85.27
	1000	-484.39	87.91	164.40	0.3340	3.949	91.90
333	Blank	-475.87	157.68	266.90	8.5191	100.690	---
	50ppm	-484.67	147.60	266.42	5.8749	68.339	
	100ppm	-480.44	114.56	226.07	4.1334	48.110	
	200ppm	-486.46	98.50	159.97	2.1812	25.780	
	500ppm	-486.44	98.23	146.51	1.346	15.910	
	1000	-486.45	100.89	158.09	0.7097	8.3800	

Tables 2a and 2b show that the corrosion current density (i_{corr}) and corrosion rate (υ_{corr}) values decreased in the presence of different concentrations of MPPMT and EPMT. The inhibition efficiency increases with an increase in concentration inhibitors, indicating that both the inhibitors successfully inhibited hydrogen evolution reaction and dissolution of metal by simply adhering to the mild steel surface and blocking the active sites. According to the reported literature [16], if the shift in the corrosion potential is more than ±85mV with respect to the corrosion potential of the blank solution, then the inhibitor is considered as either anodic or cathodic type. In the present study, the maximum displacement in corrosion potential in the presence of both the inhibitors was found to be less than ±85mV, which indicates that both the inhibitor acts as mixed indicators, preventing both cathodic and anodic reactions, i.e., the liberation of hydrogen and dissolution metal [17]. The inhibitor molecules adsorbed on the metal surface create a barrier between the metal surface and the corrosive medium, thereby protecting the metal surface from corrosion.

3.2. Temperature effect.

The study of inhibition efficiencies at different concentrations of the inhibitors at various temperatures gives useful insight into the nature of the adsorption process on the metal surface by evaluating the thermodynamic and kinetic parameters. The effect of temperature on the corrosion of mild steel in 0.5 M sulphuric acid medium in the presence of MPPMT and EPMT inhibitors was studied at a temperature range of 303 K to 333 K. The data obtained by the study indicate that the inhibition efficiencies of both the inhibitors decrease with an increase in temperature. Both MPPMT and EPMT inhibitors show maximum inhibition efficiencies at 303 K, according to PDP and EIS studies. From Tables 2a and 2b, it is found that inhibition efficiency decreased from 94.89 % to 89.87 % for MPPMT inhibitors. For EPMT the inhibition efficiency decreased from 94.56 % to 92.28 % within the temperature range from 303 K to 333 K. It can be observed from the Fig 7b that corrosion inhibition efficiencies of both the inhibitors decrease with an increase in temperature from 303 K to 333 K according to PDP studies and this is in agreement with EIS studies. The decrease in inhibition efficiencies with an increase in temperature can be due to the desorption of inhibitor molecules from the metal surface. This is also due to the roughening of the metal surface as a result of enhanced corrosion at higher temperatures. It is also observed from Figure 7a that the rate of corrosion of mild steel increases with an increase in temperature. This can be due to the increase in the conductance of the aqueous medium with an increase in the temperature, which increases the rate of diffusion of hydrogen ions to the surface of the metal [18].

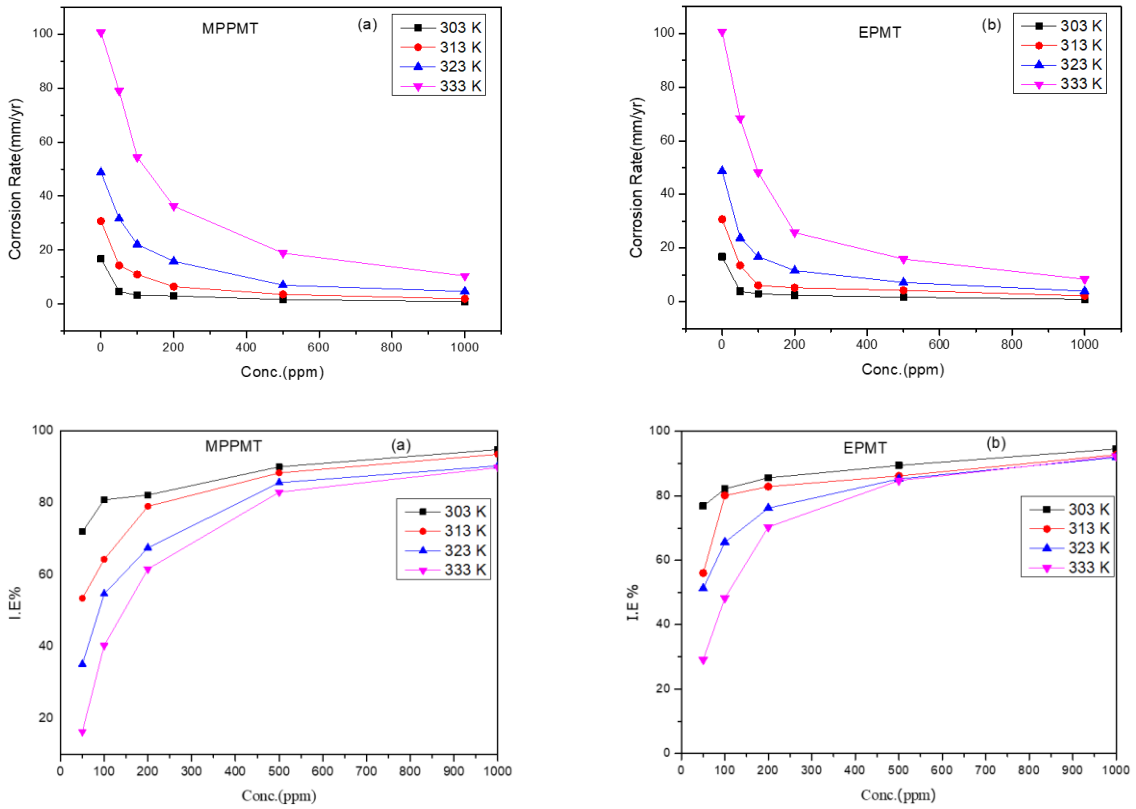

Figure 7. Plot of variation of corrosion rate and (a) inhibition efficiency with various concentrations of **(a)** MPPMT; **(b)** EPMT inhibitors.

The relation between corrosion rate and the temperature is given by the following Arrhenius Eq. (5) [19].

$$\ln CR = A - \frac{E_a}{RT} \quad (5)$$

where A is the Arrhenius constant, E_a is the energy of activation, R is the universal gas constant, and T is the absolute temperature. The plots of ln(CR) versus 1/T gave a straight line, as shown in Figure 8. The activation energy values for both the inhibitors were calculated from the slope of these lines.

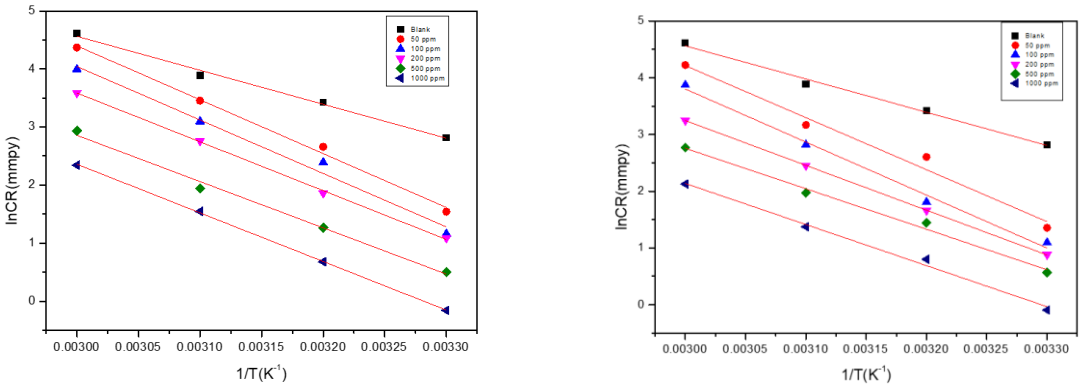

Figure 8. Arrhenius plots of lnCR vs. 1/T for MS in 0.5M sulphuric acid at different concentrations of inhibitor.

The enthalpy and entropy of activation for the corrosion MS in 0.5 M sulphuric acid for both MPPMT and EPMT were determined using the following transition state Eq. (6) [20].

$$CR = \frac{RT}{Nh}\exp\left(\frac{\Delta S^{\neq}}{R}\right)\exp\left(\frac{-\Delta H^{\neq}}{RT}\right) \quad (6)$$

where N is Avogadro's number and h is Plank's constant. Fig. 9 shows a plot of ln(CR/T) versus 1/T is a straight line with slope = ($-\Delta H^{\#}/R$) and intercept = $\ln\frac{RT}{Nh}\exp(\frac{\Delta S^{\neq}}{R})$. The activation parameter values are given in Table 3.

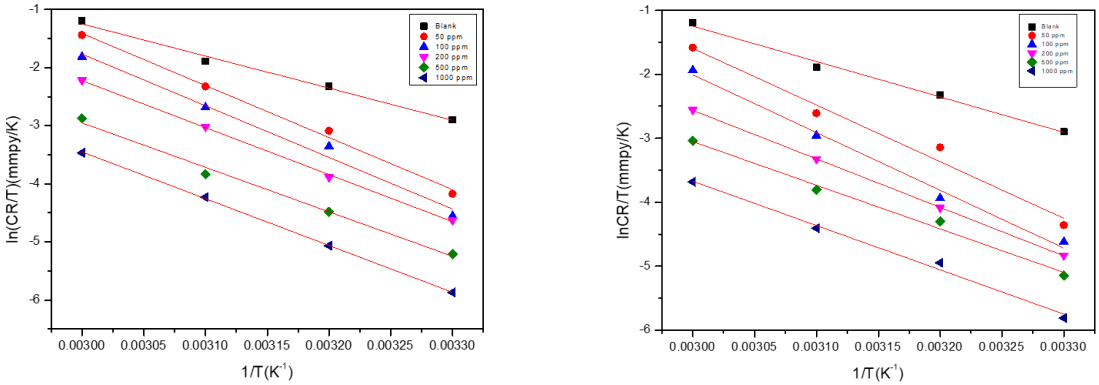

Figure 9. Plots of lnCR/T vs. 1/T for MS in 0.5 M sulphuric acid at various concentrations of inhibitor.

Table 3. Activation parameters for MS corrosion in 0.5M sulphuric acid with MPPMT and EPMT inhibitors.

Inhibitor	**Conc. of the inhibitor (ppm)**	E_a **(kJ mol^{-1})**	$\Delta H^{\neq}$ **(kJ mol^{-1})**	$\Delta S^{\neq}$ **(J mol^{-1} K^{-1})**
MPPMT	Blank	48.61	45.99	-69.90
	50	77.13	74.51	14.27
	100	76.58	73.96	9.69
	200	69.94	67.32	-14.03
	500	66.27	63.66	-31.08
	1000	69.62	67.00	-25.19
EPMT	50	76.24	73.62	10.07
	100	77.71	75.09	11.06
	200	65.65	63.03	-29.73
	500	59.31	56.69	-52.81
	1000	60.18	57.56	-55.37

Table 3 depicts the inhibitor solution's high Ea values compared to the blank solution, indicating the physical adsorption of MPPMT and EPMT on the MS surface [21]. The positive values of $\Delta H^{\#}$ suggest that the metal dissolution process is endothermic. The values of $\Delta S^{\#}$ indicate the decrease in disorder from the reactant to the activated complex state.

3.3. Adsorption isotherm.

In this study, among other isotherms, Langmuir isotherm best fits with the experimental data, and it can be concluded that the adsorption of MPPMT and EPMT inhibitors on the MS surface in H_2SO_4 follows Langmuir isotherm. The Eq. can represent Langmuir adsorption isotherm (7) [22].

$$\frac{C_{inh}}{\theta} = \frac{1}{K_{ads}} + C_{inh} \qquad (7)$$

where K_{ads} represents the adsorptive equilibrium constant, C_{inh} is the concentration of inhibitor, and θ is the degree of surface coverage.

The plot of C_{inh}/θ versus C_{inh} at various temperatures is given in Fig. 10. The free energy change ($\Delta G°_{ads}$) of adsorption was obtained from Eq. (8).

$$\Delta G^{o}_{ads} = -RT \ln(55.5 K_{ads}) \qquad (8)$$

where R is the ideal gas constant, T is the absolute temperature, and 55.5 is the molar water concentration in solution (mol/dm^3). The standard enthalpy of adsorption (ΔH^{o}_{ads}) and standard entropy of adsorption (ΔS^{o}_{ads}) are calculated from Eq. (9) [23].

$$\Delta G^{0}_{ads} = \Delta H^{o}_{ads} - T\Delta S^{o}_{ads} \qquad (9)$$

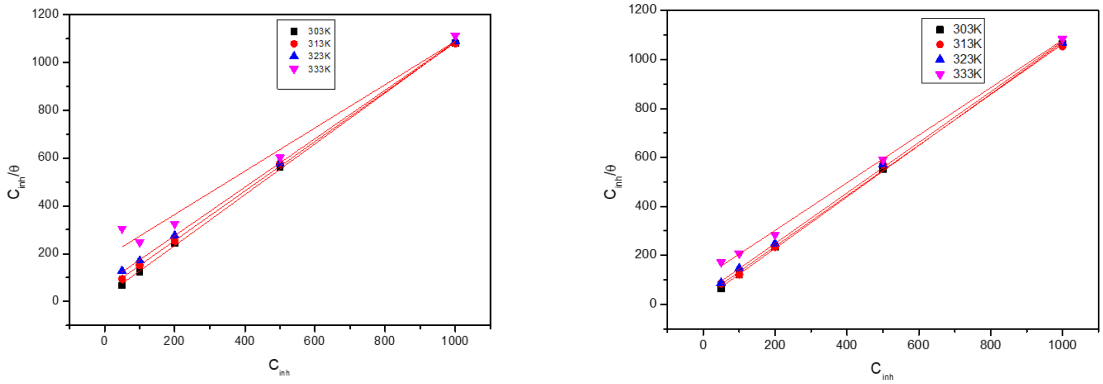

(a) **(b)**

Figure 10. Langmuir adsorption isotherms for MS in 0.5M sulphuric acid at various temperatures with **(a)** MPPMT; **(b)** EPMT.

Calculated values of K_{ads}, $\Delta G°_{ads}$, $\Delta H°_{ads}$ and $\Delta S°_{ads}$ are listed in Table 4. The negative values of $\Delta H°_{ads}$ prove that the adsorption of inhibitors is exothermic and, hence, physisorption. The negative value of ΔS^{o}_{ads} indicates the reduction in disorder from the reactant to the adsorbed species [24].

Table 4. Thermodynamic parameters for adsorption of inhibitors on mild steel at various temperatures.

Inhibitor	Temp °C	K_{ads}(M^{-1})	R^2	ΔG°_{ads} (kJ/mol)	ΔS°_{ads} (J/mol/K)	ΔH°_{ads} (kJ/mol)
MPMT	303	12324	0.9995	-33.84	-78.45	-57.64
	313	5533	0.9996	-32.87		
	323	3626	0.9999	--32.79		
	333	1443	0.9747	-31.25		
EPMT	303	15252	0.9996	-34.38	-43.7	--47.89
	313	9161	0.9982	-34.19		
	323	6512	0.9995	-34.36		
	333	2578	0.9986	-32.86		

The negative value of $\Delta G°_{ads}$ indicates that inhibitor adsorption on mild steel surfaces is spontaneous. In general, values of $\Delta G°_{ads}$ are around -20 kJ mol^{-1} or less negative, indicating physical adsorption of the indicator on the metal surface, while those higher than -40 kJ/mol indicate the chemical adsorption of the indicator on the metal surface [25]. In the present work, $\Delta G°_{ads}$ values are around -31.25 to -33.84 kJ mol^{-1} for MPPMT and -32.86 to -34.38 kJ mol^{-1} for EPMT inhibitor, suggesting that inhibitor adsorption on the mild steel surface obeys both physical and chemical adsorption mechanisms.

3.4. UV-visible spectrometry.

To confirm the formation of the Fe-Inhibitor complex, the visual absorption spectra of MPMT and EPMT inhibitors in 0.5M H_2SO_4 were recorded before and after immersion of mild steel specimen for 22 hrs at room temperature and are shown in Figures 11a and11b. According to the graph, the absorbance of the inhibitor solution before immersion of MS sample is greater than that of the inhibitor solution after immersion. The formation of the Iron-inhibitor complex caused a major change in the absorbance frequency, suggesting that the inhibitors MPPMT and EPMT adsorb on the metal surface [26].

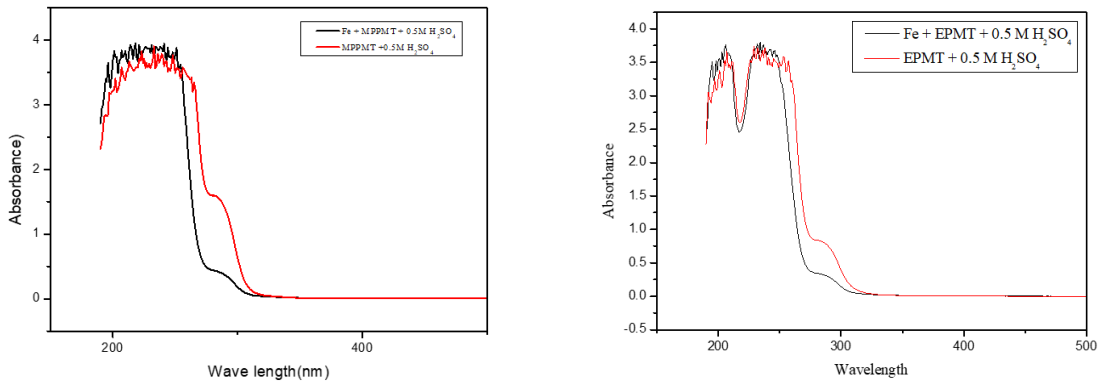

(a) **(b)**

Figure 11. UV-visible spectra of **(a)** MPMT; **(b)** EPMT inhibitor before and after immersion of mild steel sample.

3.5. FT-IR spectral analysis.

The FT-IR spectrum of MPPMT inhibitor without and with adsorption on the MS sample in 0.5 M sulphuric acid is given in Figures 12a and 12b. It can be seen that the characteristic peak at 3284 cm^{-1} for NH stretch and peak at 2941 cm^{-1} for CH stretch are displaced to the 3338 cm^{-1} and 3192 cm^{-1}, respectively, in the corrosion product. The characteristic peak for C=C stretch at 1539 cm^{-1} and the peak for C-N-C stretch at 1138 cm^{-1} displaced 1637 cm^{-1} and 1076 cm^{-1}, respectively. The FT-IR spectrum of EPMT inhibitor without and with adsorption on the MS sample in 0.5 M sulphuric acid is given in Fig. 13a and 13b. It can be seen that the characteristic peak at 3286 cm^{-1} for NH stretch and peak at 2825 cm^{-1} for CH stretch are displaced to the 3280 cm^{-1} and 2916 cm^{-1}, respectively, in the corrosion product. The characteristic peak for C=C stretch at 1544 cm^{-1} and peak for C-N-C stretch at 1155 cm^{-1} displaced to 1629 cm^{-1} and 1122 cm^{-1}, respectively, in the scratched product. Shifts in the IR frequencies in the inhibitors and the corrosion product indicate a strong interaction between the inhibitor molecules and the MS surface and the development of a protective coating on the metal [27].

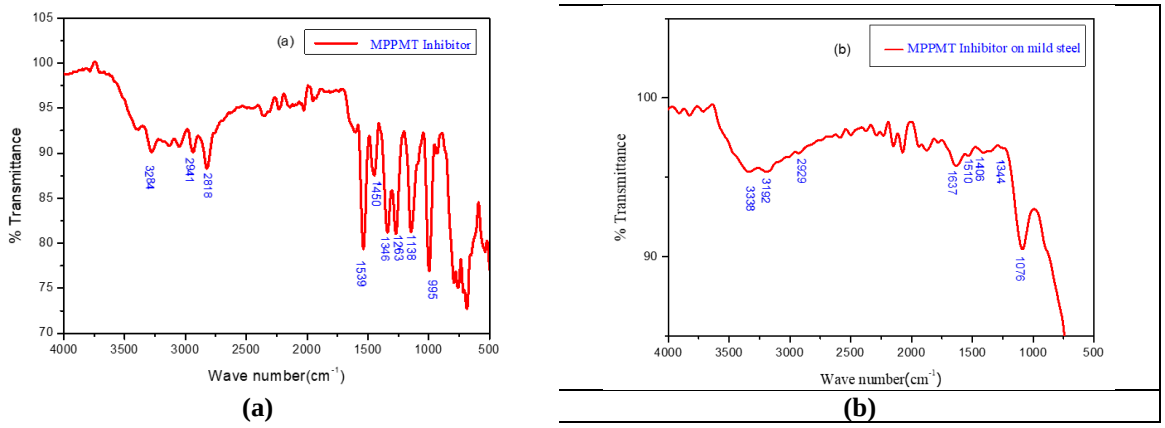

(a) **(b)**

Figure 12. FT-IR spectra of **(a)** MPPMT; **(b)** scratched MPPMT film adsorbed on MS surface.

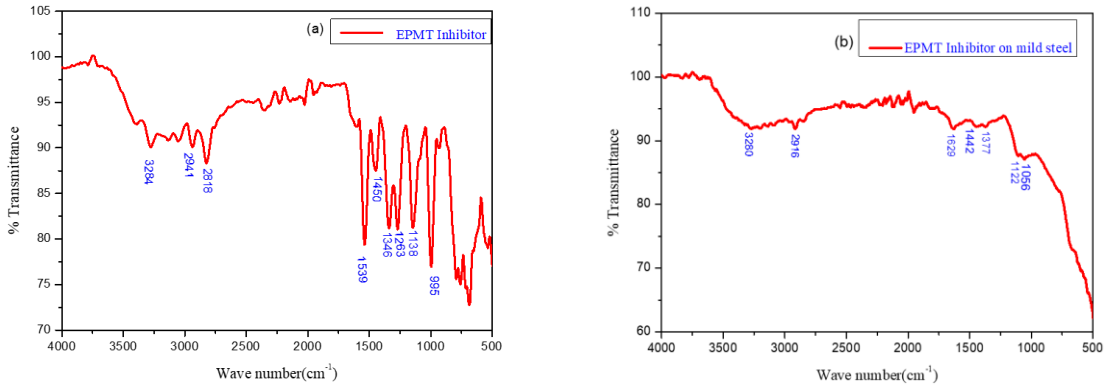

(a) **(b)**

Figure 13. FT-IR spectra of **(a)** EPMT; **(b)** scratched EPMT film adsorbed on MS surface.

3.6. Surface morphology study.

3.6.1. SEM analysis.

Micro images of MS samples dipped in 0.5M sulphuric acid for 22 hours without and with MPPMT and EPMT are given in Figure 14. Figure 14a depicts that the MS surface without the inhibitors is severely corroded, and large numbers of pits are distributed over the metal surface. Figures 14b and 14c show that the metal surface is smoother and reduces the number of pits. This indicates that the inhibitors protect the MS surface against corrosion by creating a protective coating on the metal surface when kept in 1000 ppm of MPPMT and EPMT inhibitors for 22 hours in sulphuric acid solution.

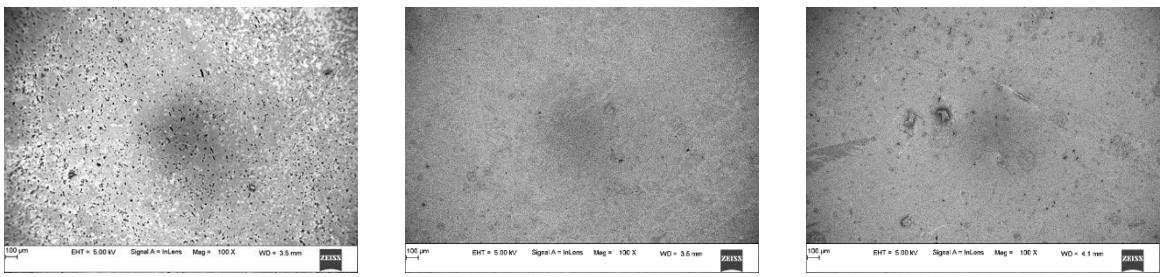

(a) **(b)** **(c)**

Figure14. Micrographs of MS specimens after dipping in 0.5M H_2SO_4 at 303 K **(a)** without inhibitor; **(b)** with 1000ppm MPPMT; **(c)** with 1000 ppm EPMT.

3.6.2. EDX analysis.

Figures 15a and 15b show the EDX spectra of MS surface in 0.5 M sulphuric acid without and with 1000 ppm MPPMT and EPMT. The spectral image of an uninhibited MS sample shows the peak of manganese, phosphorous, and silicon, indicating the corrosion of the metal in a sulphuric acid medium. These peaks are absent in the inhibited sample spectra. Table 5 shows the atomic and weight percentages of the elements obtained by the EDX image of the uninhibited and inhibited MS surfaces. The quantitative analysis found that in the corroded specimen, the atomic percentages of Iron and oxygen were 19.67 and 53.23, respectively. But in the inhibited solution containing MPPMT, the atomic percentage of Iron increased to 81.66 and oxygen reduced to 12.23, and in EPMT solution, the atomic percentage of Iron increased to 78.39 and oxygen reduced to 14.41, as given in Table 5. These findings affirm that MPPMT and EPMT inhibitors protect MS surface from corrosion by adsorbing on its surface [28].

Table 5. EDX results for corrosion of MS in the absence and presence of MPPMT and EPMT.

Element	Uninhibited sample		MPPMT		EPMT	
	Atomic %	Weight %	Atomic%	Weight%	Atomic %	Weight %
C	26.61	6.68	6.11	0.64	7.20	0.75
O	53.23	17.80	12.23	1.71	14.41	2.01
Si	0.12	0.07	-	-	-	-
P	0.25	0.16	-	-	-	-
Mn	0.12	0.14	-	-	-	-
Fe	19.67	22.96	81.66	39.88	78.39	38.14

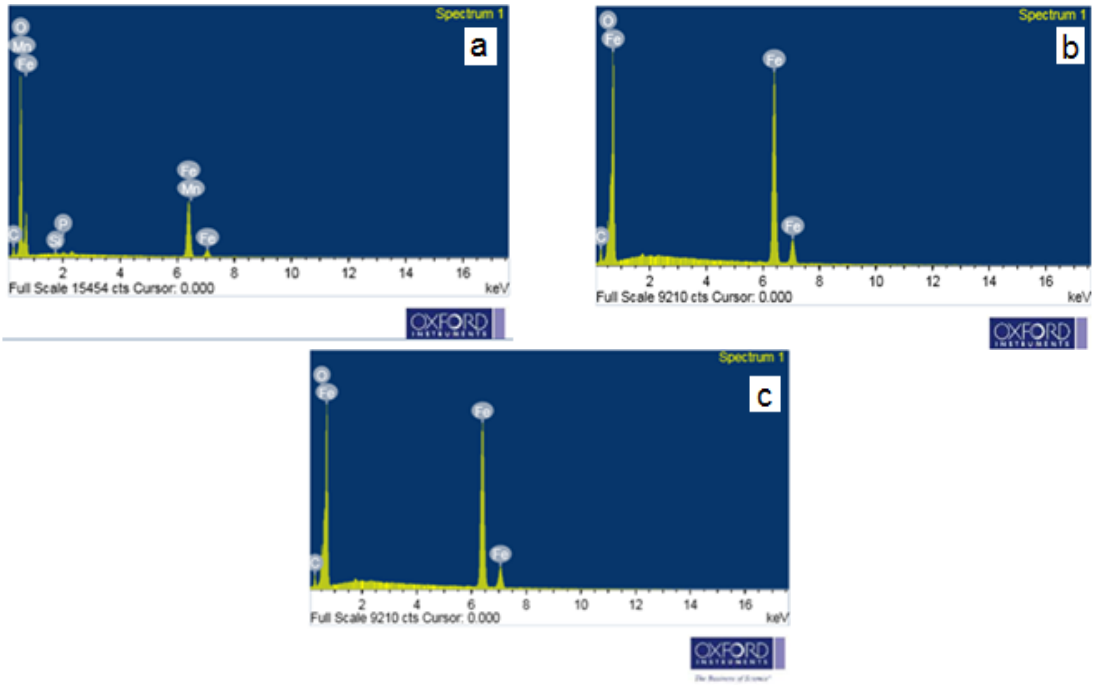

Figure 15. EDX image of MS dipped in **(a)** 0.5 M H_2SO_4; **(b)** 0.5 M H_2SO_4 with 1000 ppm MPPMT; **(c)** 0.5 M H_2SO_4 with 1000 ppm EPMT.

3.7. Quantum chemical calculations.

A DFT study explored the specific reactivity parameters and adsorption behavior of the MPPMT and EPMT inhibitors. Figures 16a and 16b show the ground state geometry structure, HOMO, and LUMO images of MPPMT and EPMT, respectively. The parameters of the theoretical calculations, such as the highest occupied molecular orbital energy(E_{HOMO}), the lowest unoccupied molecular orbital energy (E_{LUMO}), electron affinity (A), ionization potential

(I), chemical softness or electron polarizability (σ,) chemical hardness (η), electrophilicity index (ω), electronegativity (χ) and chemical potential (μ) are tabulated in Table 6. E_{HOMO} relates to the electron-giving ability of the molecule, and E_{LUMO} represents the electron acceptance ability of the donor species. The inhibitor with a large E_{HOMO} value has the highest tendency to donate electrons to the species with empty molecular orbitals [29].

According to Koopman's theorem, ionization energy and electron affinity are related to energies of the molecular orbitals and are calculated by Eq. (10) and (11).

$$-E_{HOMO} = I \quad (10)$$

$$-E_{LUMO} = A \quad (11)$$

Where I denote the ionization energy and A denotes the electron affinity. Chemical hardness(η) and softness(σ) are obtained from ionization energy and electron affinity using Eq. (12) and (13) [30]. These are related to corrosion inhibition and are focused on Lewis acids and bases theory and Pearson's concept of hard and soft acids and bases [31].

$$\eta = \frac{1}{2}(I - A) \quad (12)$$

$$\sigma = {}^{1}/_{\eta} \quad (13)$$

The electronic chemical potential μ is given by Eq. 14.

$$\mu = -\frac{(I+A)}{2} \quad (14)$$

Electronegativity (χ) and electrophilicity index (ω) were calculated using Eq. (15) and Eq. (16) [32,33]. A good electrophile is denoted by its high electrophilicity value, and a good nucleophile has a low electrophilicity value.

$$\chi = \frac{1}{2}(I + A) \quad (15)$$

$$\omega = {}^{\mu^2}/_{2\eta} \quad (16)$$

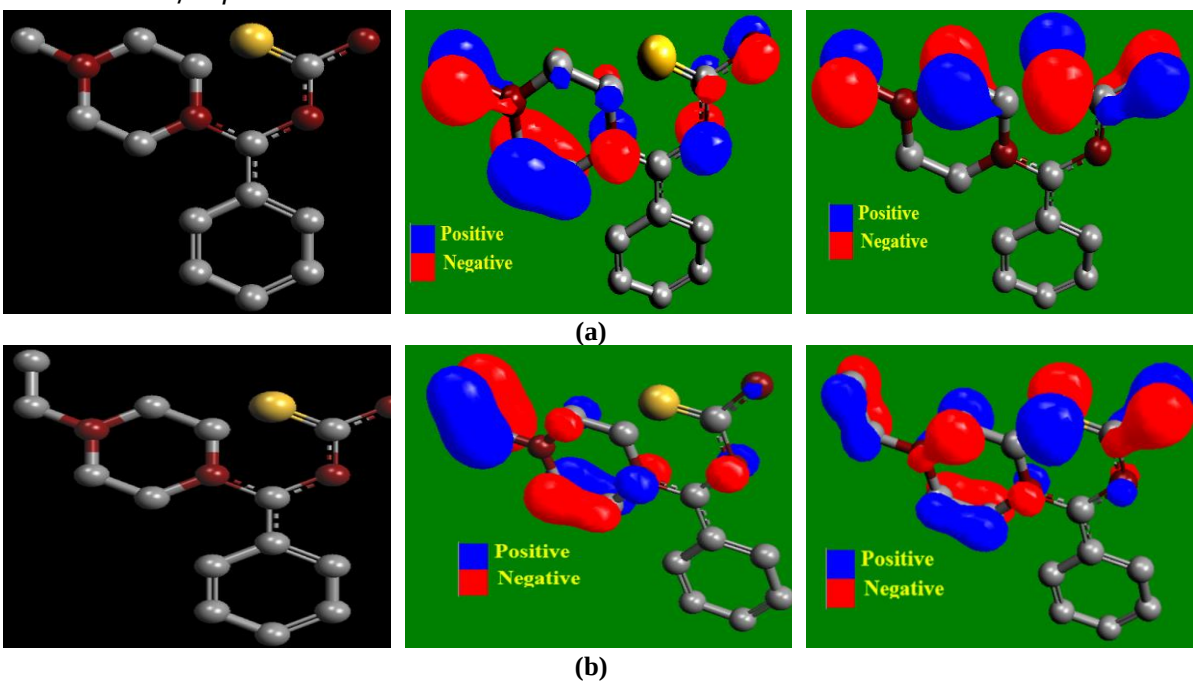

Figure 16. (a) Ground state geometry structure, HOMO and LUMO of MPPMT; **(b)** Ground state geometry structure, HOMO and LUMO of EPMT.

Table 6. Quantum chemical parameters of MPPMT and EPMT.

Inhibitor	HOMO (eV)	LUMO (eV)	ΔE (eV)	I (eV)	A (eV)	η (eV)	χ (eV)	σ $(eV)^{-1}$	μ (eV)	ω (eV)
MPPMT	-8.3928	-3.9776	4.4151	8.392	3.977	2.207	6.185	0.452	-6.185	8.664

Inhibitor	HOMO (eV)	LUMO (eV)	ΔE (eV)	I (eV)	A (eV)	η (eV)	χ (eV)	σ $(eV)^{-1}$	μ (eV)	ω (eV)
EPMT	-9.0875	-4.6059	4.4816	9.087	4.605	2.240	6.846	0.446	-6.846	10.459

The results in Table 6 indicate that $-E_{HOMO}$ value of both MPPMT and EPMT is greater than their $-E_{LUMO}$ value, indicating that both the inhibitor has a high electron-donating and high electron-accepting ability, resulting in strong bonding between the inhibitor molecules and the MS surface. The smaller energy gap of the MPPMT and EPMT inhibitors indicates the high reactivity of the inhibitors and strong bonding between the inhibitor molecules and the MS surface [34].

3.8. Mechanism of inhibition.

The chemical structure of the inhibitor molecule, the charge on the metal surface, and the type of interaction with the metal surface influence the adsorption phenomenon. In the present study from the $\Delta G°_{ads}$, it is evident that the adsorption of both MPPMT and EPMT inhibitors on the metal surface takes place through both physisorption and chemisorption. Chemical adsorption occurs by interacting with an unshared pair of electrons on oxygen, sulfur, nitrogen atoms, and π- electrons of the un-protonated inhibitor with vacant d-orbital of mild steel. In acid, medium metal bears a positive charge; therefore, chloride ions of hydrochloric acid adsorb onto the metal surface, creating a negative charge on the mild steel surface. So, physical adsorption occurs through the electrostatic interaction between the protonated inhibitor molecules and the oppositely charged mild steel surface, promoting physisorption [35]. The formation of an adsorptive layer on the corroding surface of steel through physical and chemical adsorption causes a decrease in the corrosion rate. An increase in inhibitor concentration covers a larger surface area and increases inhibition efficiency.

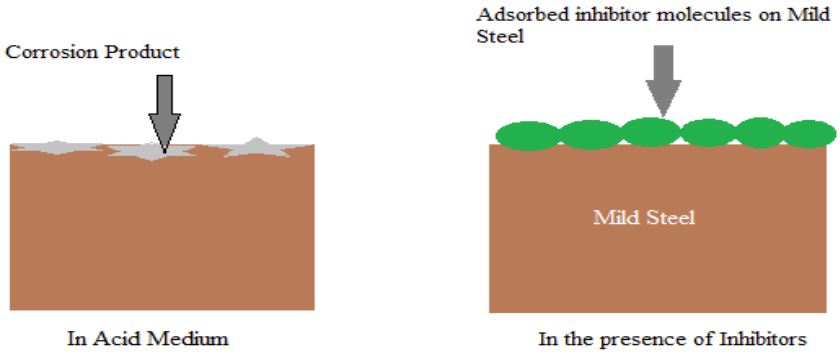

Figure 15. Schematic representation of adsorption of inhibitor molecules on mild steel surface.

4. Conclusion

In conclusion, this study has demonstrated the effectiveness of both MPPMT and EPMT as potent inhibitors of mild steel corrosion in a 0.5M H_2SO_4 medium. The inhibitor efficiency was found to increase with higher concentrations, reinforcing their utility in corrosion prevention strategies. Polarization studies confirmed that these inhibitors function as mixed-type inhibitors, adhering to the Langmuir adsorption isotherm model, which emphasizes their adsorption behavior's predictable and consistent nature.

Electrochemical impedance spectroscopy further supported these findings, revealing a significant increase in charge transfer resistance as the concentration of the inhibitors rose, indicating enhanced surface protection. The inhibitory mechanism, attributed to both physical and chemical adsorption processes, was validated through the activation and thermodynamic

parameters derived from the experiments. These results suggest a dual mechanism that enhances the robustness of the inhibition process.

Additionally, surface morphology analysis using SEM and EDX confirmed the adsorption of the inhibitors onto the MS surface, providing visual and compositional evidence for their effectiveness. Importantly, the strong correlation between the experimental results from electrochemical studies and the quantum chemical analysis highlights the reliability and consistency of the findings.

Overall, this research underscores the potential of MPPMT and EPMT as effective inhibitors for MS corrosion in acidic environments. The alignment of electrochemical and quantum chemical data reinforces the conclusion that these inhibitors offer a promising solution for extending the longevity of metal components in corrosive conditions. Future studies could explore these inhibitors' scalability and long-term performance in industrial applications.

Funding

This research received no external funding.

Acknowledgments

Declared none.

Conflict of interest

The authors declare no conflict of interest.

References

1. Acidi, A.; Sedik, A.; Rizi, A.; Bouasla, R.; Rachedi, K.O.; Berredjem, M.; Delimi, A.; Abdennouri, A.; Ferkous, H.; Yadav, K.K.; Alam, M.; Ernst, B.; Bengureba, Y. Examination of the main chemical components of essential oil of *Syzygium aromaticum* as a corrosion inhibitor on the mild steel in 0.5 M HCl medium. *J. Mol. Liq.* **2023**, *391*, 123423, https://doi.org/10.1016/j.molliq.2023.123423.
2. Al Kiey, S.A.; Mohamed-Ezzat, R.A.; Dacrory, S. Eco-friendly anti-corrosion performance of chitosan modified with fused heterocyclic compound on mild steel in acidic medium. *Int. J. Biol. Macromol.* **2024**, *263*, 130133, https://doi.org/10.1016/j.ijbiomac.2024.130133.
3. Betti, N.; Al-Amiery, A.A.; Al-Azzawi, W.K.; Isahak, W.N.R.W. Corrosion inhibition properties of schiff base derivative against mild steel in HCl environment complemented with DFT investigations. *Sci. Rep.* **2023**, *13*, 8979, https://doi.org/10.1038/s41598-023-36064-w.
4. Lavanya, D.K.; Priya Frank, V.; Vijaya, D.P. Corrosion Inhibitive Effect of Novel Eco Friendly Corrosion Inhibitors for Mild Steel in 0.5 M HCl—A Comparative Study. *Surf. Eng. Appl. Electrochem.* **2020**, *56*, 524-532, https://doi.org/10.3103/S1068375520040080.
5. Boudalia, M.; Fernández-Domene, R.M.; Guo, L.; Echihi, S.; Belghiti, M.E.; Zarrouk, A.; Bellaouchou, A.; Guenbour, A.; García-Antón, J. Experimental and Theoretical Tests on the Corrosion Protection of Mild Steel in Hydrochloric Acid Environment by the Use of Pyrazole Derivative. *Materials* **2023**, *16*, 678, https://doi.org/10.3390/ma16020678.
6. Bangera, S.; Alva, V.D.P. Aqueous Extract of Macaranga Peltata Leaves—Green Corrosion Inhibitor for Mild Steel in Hydrochloric Acid Medium. *Surf. Eng. Appl. Electrochem.* **2020**, *56*, 259–266, https://doi.org/10.3103/S1068375520020040.
7. Sunil, D.; Kumari, P.; Shetty, P.; Rao, S.A. Indole Hydrazide Derivatives as Potential Corrosion Inhibitors for Mild Steel in HCl Acid Medium: Experimental Study and Theoretical Calculations. *Trans. Indian Inst. Met.* **2022**, *75*, 11–25, https://doi.org/10.1007/s12666-021-02382-8.
8. Rasheeda, K.; Alamri, A.H.; Krishnaprasad, P.A.; Swathi, N.P.; Alva, V.D.; Aljohani, T.A. Efficiency of a pyrimidine derivative for the corrosion inhibition of C1018 carbon steel in aqueous acidic medium:

Experimental and theoretical approach. *Colloids Surf. A Physicochem. Eng. Asp.* https://doi.org/10.1016/j.colsurfa.2022.128631.

9. Meddings, N.; Heinrich, M.; Overney, F.; Lee, J.-S.; Ruiz, V.; Napolitano, E.; Seitz, S.; Hinds, G.; Raccichini, R.; Gaberšček, M.; Park, J. Application of electrochemical impedance spectroscopy to commercial Li-ion cells: A review. *J. Power Sources.* **2020**, *480*, 228742, https://doi.org/10.1016/j.jpowsour.2020.228742.
10. Rasheeda, K.; Swathi, N.P.; Alva, V.D.P.; Samshuddin, S.; Aljohani, T.A.; Baig, I.; Alomari, F.Y.; Alamri, A.H. Applicability of some new pyrimidine derivatives for the corrosion inhibition of mild steel in the acidic environment. *S. Afr. J. Chem. Eng.* **2024**, *48*, 80-94, https://doi.org/10.1016/j.sajce.2024.01.006.
11. Swathi, N.P.; Samshuddin, S.; Alamri, A.H.; Rasheeda, K.; Alva, V.D.P.; Aljohani, T.A. Experimental and theoretical investigation of a new triazole derivative for the corrosion inhibition of carbon steel in acid medium. *Egypt. J. Pet.* **2022**, *31*, 15-21, https://doi.org/10.1016/j.ejpe.2022.04.002.
12. Ergun, Ü.; Yüzer, D.; Emregül, K.C. The inhibitory effect of bis-2,6-(3,5-dimethylpyrazolyl)pyridine on the corrosion behaviour of mild steel in HCl solution. *Mater. Chem. Phys.* **2008**, *109*, 492–499, https://doi.org/10.1016/j.matchemphys.2007.12.023.
13. Gholami, M.; Danaee, I.; Maddahy, M.H.; RashvandAvei, M. Correlated ab Initio and Electroanalytical Study on Inhibition Behavior of 2-Mercaptobenzothiazole and Its Thiole–Thione Tautomerism Effect for the Corrosion of Steel (API 5L X52) in Sulphuric Acid Solution. *Ind. Eng. Chem. Res.* **2013**, *52*, 14875–14889, https://doi.org/10.1021/ie402108g.
14. Hegazy, M.A.; Abdallah, M.; Awad, M.K.; Rezk, M. Three novel di-quaternary ammonium salts as corrosion inhibitors for API X65 steel pipeline in acidic solution. Part I: Experimental results. *Corros. Sci.* **2014**, *81*, 54–64, https://doi.org/10.1016/j.corsci.2013.12.010.
15. Gadow, H.S.; Fakeeh, M. Green inhibitor of carbon steel corrosion in 1 M hydrochloric acid: *Eruca sativa* seed extract (experimental and theoretical studies). *RSC Adv.* **2022**, *12*, 8953-8986, https://doi.org/10.1039/D2RA01296K.
16. Lavanya, D.K.; Priya, F.V.; Vijaya, D.P. Green Approach to Corrosion Inhibition of Mild Steel in Hydrochloric Acid by 1-[Morpholin-4-yl (thiophen-2-yl) methyl] thiourea. *J. Fail. Anal. Preven.* **2020**, *20*, 494-502, https://doi.org/10.1007/s11668-020-00850-9.
17. Ali, H.A.; Shaban, M.M.; Abousalem, A.S.; Ghaith, E.A.; Fouda, A.S.; Ismail, M.A. Novel biphenylidene-thiopyrimidine derivatives as corrosion inhibitors for carbon-steel in oilfield produced water. *Sci. Rep*. **2023**, *13*, 16388, https://doi.org/10.1038/s41598-023-43312-6.
18. Chen, Y.; Chen, Z.; Zhuo, Y. Newly Synthesized Morpholinyl Mannich Bases as Corrosion Inhibitors for N80 Steel in Acid Environment. *Materials* **2022**, *15*, 4218, https://doi.org/10.3390/ma15124218.
19. Pinto, V.; Pinto, G.M.; Kateel, L.D.; Thomas, A. Green Approach to Corrosion Inhibition of Mild Steel in Hydrochloric Acidusing Extractfromthe Pericarp of the fruit *Tamarindus indica* (Tamarind). *Biointerface Res. Appl. Chem*. **2023**, *13*, 544, https://doi.org/10.33263/BRIAC136.544.
20. Hegde, M.; Nayak, S.P.; Raghavendra, N. Microwave-assisted extraction of Swietenia macrophylla fruit shell and its application in corrosion inhibition for mild steel in 0.5 M HCl pickling environment. *Sādhanā* **2023**, *48*, 10, https://doi.org/10.1007/s12046-022-02066-z.
21. Noor, E.A.; Al-Moubaraki, A.H. Thermodynamic study of metal corrosion and inhibitor adsorption processes in mild steel/1-methyl-4[4′(-X)-styryl pyridinium iodides/hydrochloric acid systems. *Mater. Chem. Phys*. **2008**, *110*, 145–154, https://doi.org/10.1016/j.matchemphys.2008.01.028.
22. Yousif, Q.A.; Fadel, Z.; Abuelela, A.M.; Alosaimi, E.H.; Melhi, S.; Bedair, M.A. Insight into the corrosion mitigation performance of three novel benzimidazole derivatives of amino acids for carbon steel (X56) in 1 M HCl solution. *RSC Adv.* **2023**, *13*, 13094-13119, https://doi.org/10.1039/D3RA01837G.
23. Vinutha, M.R.; Venkatesha, T.V.; Nagaraja, C. Anticorrosive ability of electrochemically synthesized 2,2′-disulfanediyldianiline for mild steel corrosion: electrochemical and thermodynamic studies. *Int. J. Ind. Chem.* **2018**, *9*, 185–197, https://doi.org/10.1007/s40090-018-0149-0.
24. Shetty, D.; Preethi Kumari, P.; Rao, S.A.; Shetty, P. Anticorrosion Behaviour of a Hydrazide Derivative on 6061 Al-15%(v) SiC(P) Composite in Acid Medium: Experimental and Theoretical Calculations. *J. Bio-Tribo-Corros.* **2020**, *6*, 59, https://doi.org/10.1007/s40735-020-00356-9.
25. Chaouiki, A.; Chafiq, M.; Ko, Y.G.; Al-Moubaraki, A.H.; Thari, F.Z.; Salghi, R.; Karrouchi, K.; Bougrin, K.; Ali, I.H.; Lgaz, H. Adsorption Mechanism of Eco-Friendly Corrosion Inhibitors for Exceptional Corrosion Protection of Carbon Steel: Electrochemical and First-Principles DFT Evaluations. *Metals* **2022**, *12*, 1598, https://doi.org/10.3390/met12101598.

26. Haldhar, R.; Prasad, D.; Saxena, A. *Myristica fragrans* extract as an eco-friendly corrosion inhibitor for mild steel in 0.5 M H_2SO_4 solution. *J. Environ. Chem. Eng.* **2018**, *6*, 2290–2301, https://doi.org/10.1016/j.jece.2018.03.023.
27. Fouda, A.S.; El-Haddad, M.N.; Ismail, M.A.; Abd Elgyed, A. Investigation of 6-[5-(4-Methoxyphenyl) furan-2-yl] Nicotinonitrile as a New Corrosion Inhibitor for Carbon Steel in Acidic Solution: Chemical, Electrochemical and Quantum Chemical Studies. *J. Bio- Tribo- Corros.* **2019**, *5*, 73, https://doi.org/10.1007/s40735-019-0265-1.
28. Chafiq, M.; Chaouiki, A.; Lgaz, H.; Salghi, R.; Gaonkar, S.L.; Bhat, K.S.; Marzouki, R.; Ali, I.H.; Khan, M.I.; Shimizu, H.; Chung, I.-M. Synthesis and corrosion inhibition evaluation of a new schiff base hydrazone for mild steel corrosion in HCl medium: electrochemical, DFT, and molecular dynamics simulations studies. *J. Adhes. Sci. Technol.* **2020**, *34*, 1283–1314, https://doi.org/10.1080/01694243.2019.1707561.
29. Lavanya, D.K.; Priya Frank, V.; Vijaya, D.P.; Bangera, S. Inhibition Effect of Thiourea Derivative for Mild Steel Corrosion in Acid Medium: Experimental and Theoretical Studies. *J. Bio- Tribo- Corros.* **2021**, *7*, 47, https://doi.org/10.1007/s40735-021-00487-7.
30. Peme, T.; Olasunkanmi, L.O.; Bahadur, I.; Adekunle, A.S.; Kabanda, M.M.; Ebenso, E.E. Adsorption and Corrosion Inhibition Studies of Some Selected Dyes as Corrosion Inhibitors for Mild Steel in Acidic Medium: Gravimetric, Electrochemical, Quantum Chemical Studies and Synergistic Effect with Iodide Ions. *Molecules* **2015**, *20*, 16004–16029, https://doi.org/10.3390/molecules200916004.
31. Kagatikar, S.; Sunil, D.; Kumari, P.; Shetty, P. Investigation of Anticorrosive Property of Carbazolecarbaldehyde Azine on Mild Steel Using Electrochemical, Morphological and Theoretical Studies. *J. Bio- Tribo- Corros.* **2020**, *6*, 136, https://doi.org/10.1007/s40735-020-00433-z.
32. Kateel, L.D.; Frank, P.V.; Alva, V.D.P. Corrosion Inhibition of Mild Steel in Hydrochloric Acid Medium Using Schiff Base Synthesized by Green Approach. *Surf. Eng. Appl. Electrochem.* **2023**, *59*, 511-522, https://doi.org/10.3103/S106837552304004X.
33. Swathi, N.P.; Samshuddin, S.; Aljohani, T.A.; Rasheeda, K.; Alva, V.D.P.; Alomari, F.Y.; Alamri, A.H. A new 1,2,4-triazole derivative as an excellent corrosion inhibitor: Electrochemical experiments with theoretical validation. *Mater. Chem. Phys.* **2022**, *291*, 126677, https://doi.org/10.1016/j.matchemphys.2022.126677.
34. Lgaz, H.; Saha, S.K.; Chaouiki, A.; Bhat, K.S.; Salghi, R.; Shubhalaxmi; Banerjee, P.; Ali, I.H.; Khan, M.I.; Chung, I.-M. Exploring the potential role of pyrazoline derivatives in corrosion inhibition of mild steel in hydrochloric acid solution: Insights from experimental and computational studies. *Constr. Build. Mater.* **2020**, *233*, 117320, https://doi.org/10.1016/j.conbuildmat.2019.117320.
35. Pavithra, N.S.; Alva, V.D.P.; Bangera, S. A Sustainable and Green Approach to Corrosion Inhibition of Mild Steel by Rangoon Creeper Flower Extract in 1 M HCl. *Surf. Eng. Appl. Electrochem.* **2021**, *57*, 455–465, https://doi.org/10.3103/S106837552104013X.